

Adaptive Learned Image Compression with Graph Neural Networks

Yunuo Chen¹ Bing He¹ Zezheng Lyu² Hongwei Hu³ Qunshan Gu³ Yuan Tian⁴ Guo Lu^{1*}
¹Shanghai Jiao Tong University ²Massachusetts Institute of Technology
³Alibaba Group ⁴Shanghai AI Laboratory

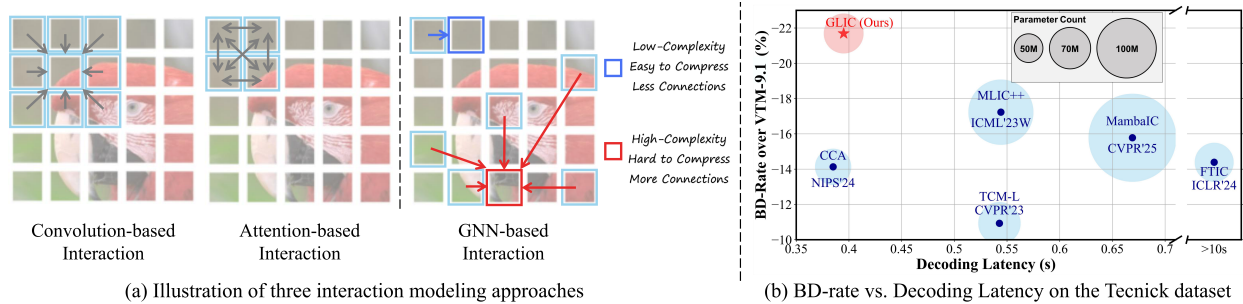


Figure 1. (a) While standard convolution and window attention-based methods are constrained by a rigid local window and a fixed connectivity pattern, our GNN-based interactions enable local and global adaptive connections across the image. (b) Rate-Distortion performance and efficiency comparisons on the Tecnick dataset. Upper left is better.

Abstract

Efficient image compression relies on modeling both local and global redundancy. Most state-of-the-art (SOTA) learned image compression (LIC) methods are based on CNNs or Transformers, which are inherently rigid. Standard CNN kernels and window-based attention mechanisms impose fixed receptive fields and static connectivity patterns, which potentially couple non-redundant pixels simply due to their proximity in Euclidean space. This rigidity limits the model’s ability to adaptively capture spatially varying redundancy across the image, particularly at the global level. To overcome these limitations, we propose a content-adaptive image compression framework based on Graph Neural Networks (GNNs). Specifically, our approach constructs dual-scale graphs that enable flexible, data-driven receptive fields. Furthermore, we introduce adaptive connectivity by dynamically adjusting the number of neighbors for each node based on local content complexity. These innovations empower our Graph-based Learned Image Compression (GLIC) model to effectively model diverse redundancy patterns across images, leading to more efficient and adaptive compression. Experiments demonstrate that GLIC achieves state-of-the-art performance, achieving BD-rate reductions of 19.29%, 21.69%, and 18.71% relative to VTM-9.1 on Kodak, Tecnick, and CLIC, respectively. Code will be released at <https://github.com/UnoC-727/GLIC>.

* Corresponding author

1. Introduction

With the exponential growth of digital image data, efficient image compression has become indispensable. Lossy compression addresses this need by significantly reducing file sizes while maintaining acceptable visual quality, thereby optimizing storage and transmission efficiency. Recent advancements in learned image compression have demonstrated remarkable potential as an alternative to traditional codecs [3, 4, 10, 29, 41, 57, 58, 80]. By leveraging advanced nonlinear transforms for encoding and decoding, both CNN-based and transformer-based LIC models have achieved superior rate-distortion performance [28, 38, 47]. Due to the quadratic complexity of transformers, recent studies commonly adopt window attention to preserve efficiency [9, 37].

However, a fundamental limitation persists: standard CNNs and window attention impose a fixed receptive field and a static connectivity pattern. As illustrated in Fig. 1 (a), a $k \times k$ convolution invariably connects each pixel to its fixed k^2 neighbors, while window attention also operates within preset blocks. Such rigidity not only prevents the network from expanding its receptive field for distant redundancy, but also tends to couple unrelated features that merely fall inside the same Euclidean neighborhood. Moreover, natural images exhibit highly non-uniform redundancy: smooth regions carry little information (high redundancy), whereas textured or edge-rich areas contain far more information (low redundancy). Constrained by static connectivity, standard CNN- and Transformer-based LIC models therefore struggle

to adapt efficiently to this spatially varying redundancy.

To overcome this limitation, we turn to Graph Neural Networks (GNNs), whose dynamic, data-dependent connectivity naturally captures non-Euclidean relationships beyond fixed Euclidean neighborhoods [21, 56]. These properties make GNNs a compelling foundation for learned image compression, where redundancy is spatially varying and long-range correlations are common. Building on this insight, we introduce a content-adaptive, Graph-based Feature Aggregation (GFA) block that fuses two complementary strategies. First, we design *dual-scale graphs* that jointly leverage a dense local graph and a sparse global graph to capture short- and long-range dependencies with near-linear complexity. By selecting connected nodes from both graphs, the network can flexibly adapt its receptive field across the image, preserving fine details while exploiting distant correlation. Second, we propose an *adaptive-degree* mechanism that assigns each node a data-driven neighbor quota based on a complexity-aware scoring function, enabling pixel-wise variable neighborhood sizes. This content-adaptive connectivity allocates more capacity to structurally complex regions while avoiding over-connection in smooth areas, improving the model’s ability to identify and eliminate redundancy.

Together, these two strategies yield a simple yet effective route for content-adaptive redundancy removal in LIC models: dual-scale candidate sampling determines the optimal *where* to connect, and adaptive degree determines *how much* to connect. As shown in Fig. 1(b), integrating our GFA block brings significant performance gains over recent strong baselines while maintaining high efficiency.

Our main contributions are summarized as follows:

- We construct dual-scale graphs to enable flexible receptive fields, allowing each pixel to select relevant nodes from both neighborhood and distant regions.
- We propose a complexity-aware scoring mechanism that evaluates compressibility and dynamically determines the optimal connection degree for each node.
- We present our GNN-based LIC model, GLIC, which outperforms VTM-9.1 by -19.29%, -21.69% and -18.71% in BD-rate on the Kodak, Tecnick, and CLIC datasets.

2. Related Work

2.1. Learned Image Compression

End-to-end learned image compression has advanced significantly in recent years and some works explore LLMs and Diffusion models for extreme and semantic compression [12, 14, 16, 19, 44, 45, 49, 67, 68, 82]. Ballé *et al.* [3] pioneered the first CNN-based LIC model, and their subsequent integration of VAEs with hyper-priors [4] established a foundational framework. Building on this, research has primarily targeted two core components to improve rate-distortion performance: transform networks and entropy

models [1, 5, 17, 20, 30, 51, 53, 55, 71, 78, 81]. Transform design has seen innovations like residual blocks [13], octave [8] and invertible networks [72]. Transformers gained prominence via Swin variants [84, 85], CNN-Transformer hybrids [9, 47], and frequency-based attention [37]. Some methods [11, 61, 79] achieve linear modeling with Mamba. Entropy modeling advanced with autoregressive [58], checkerboard [26], channel-wise [57] alongside quadrees [39, 40], Transformers [60], and multi-reference frameworks [29, 31]. T-CA [37] further improved channel-wise modeling.

Recent works explore dynamic, content-adaptive architectures for LIC, such as deformable convolutions and graph neural networks (GNNs). Deformable convolutions, applied in image/video compression [18, 36, 70], suffer from limited offset ranges. GNN-based methods face challenges: some [65, 75] scale poorly due to quadratic complexity, while others [64] are restricted by local receptive fields.

2.2. Graph Neural Network

Graph neural networks (GNNs) and graph convolution networks (GCNs) were first introduced in [21] and [56], providing a framework for processing graph-structured data. These models have been widely adopted in computer vision tasks, both for 2D and 3D data. In 3D applications, GNNs and GCNs have been applied to point cloud classification, scene graph generation, and action recognition [32, 35, 73, 74, 76]. For 2D tasks, GCNs are effective in image classification, object detection, and semantic segmentation [22, 24, 54], where they help capture spatial relationships and contextual dependencies. Additionally, GNNs and GCNs have shown promise in low-level vision tasks such as image denoising and super-resolution, where images are treated as graphs to enhance performance [42, 48, 59, 66, 83].

3. Method

3.1. Preliminary

Fig. 2 (a) shows a standard LIC pipeline with an *Encoder* g_a , a *Decoder* g_s , and an *Entropy Model*. The encoder maps an RGB image x to a latent y , which is quantized into \hat{y} and decoded to the reconstruction \hat{x} :

$$y = g_a(x; \theta_a), \hat{y} = Q(y - \mu) + \mu, \hat{x} = g_s(\hat{y}; \theta_s).$$

To estimate the entropy parameters (μ, σ) , a *Hyper Encoder-Decoder* pair converts y to side-information \hat{z} :

$$z = h_a(y; \phi_a), \hat{z} = Q(z), (\mu, \sigma) = h_s(\hat{z}; \phi_s).$$

Training minimizes the rate-distortion objective

$$\mathcal{L} = \mathcal{R}(\hat{y}) + \mathcal{R}(\hat{z}) + \lambda \mathcal{D}(x, \hat{x}),$$

where $\mathcal{R}(\cdot)$ is the predicted bitrate, $\mathcal{D}(\cdot, \cdot)$ the distortion metric, and λ balances rate against reconstruction quality.

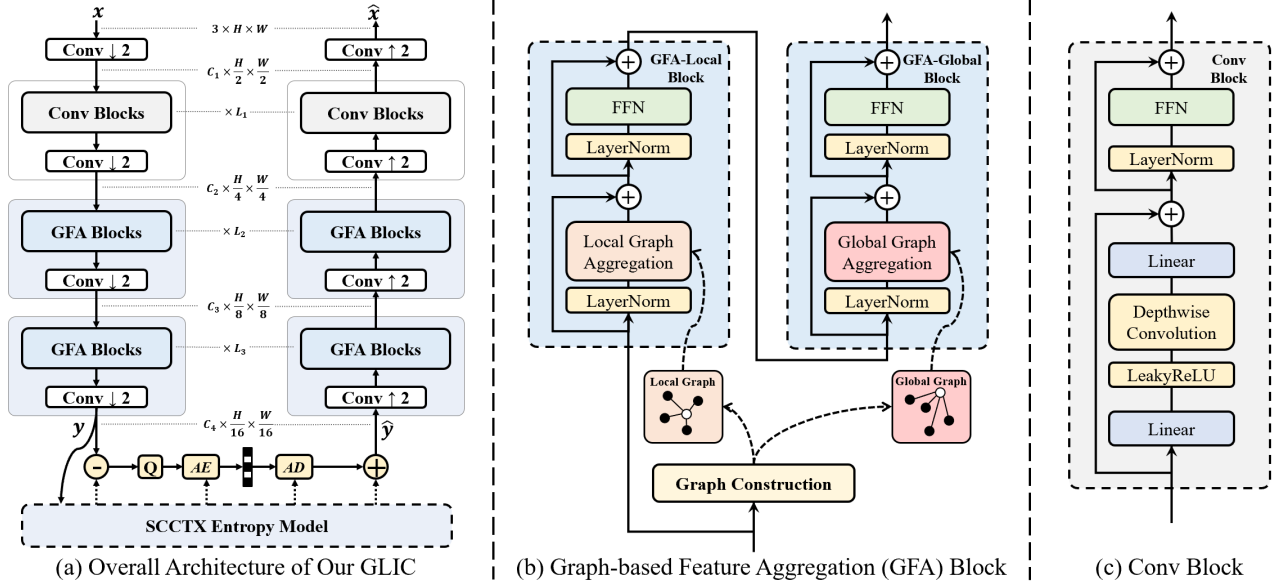


Figure 2. **Overview of our method.** (a) Architecture of the proposed GLIC codec. Channel widths are C_1, C_2, C_3, C_4 , and the numbers of non-linear transform blocks are L_1, L_2, L_3 . (b) Graph-based Feature Aggregation Block used as advanced non-linear transforms. (c) Lightweight Conv Block for early feature extraction and reduced complexity.

3.2. Overview of Our Method

As shown in Fig. 2, our Graph-based Learned Image Compression (GLIC) model adopts a standard VAE-based LIC backbone. We divide the nonlinear transforms into three stages by spatial-resolution and deploy our *Graph-based Feature Aggregation* (GFA) block in the latter two stages. Within each stage, features are aggregated sequentially by GFA-Local and GFA-Global blocks with dual-scale graphs.

At a high level, each GFA stage (i) forms a dual-scale candidate set per node to realize flexible receptive fields; (ii) assigns a complexity-aware degree budget driven by an RMS-Gradient score; (iii) constructs a directed graph by per-node thresholding with a bisection search; and (iv) performs edge-conditioned aggregation for feature updating.

3.3. Graph-based Feature Aggregation (GFA) Block

Let $F \in \mathbb{R}^{H \times W \times C}$ be a feature map with $N = H \times W$ pixels. We index feature pixels (and thus graph nodes) by $i \in \{1, \dots, N\}$ and denote the one-to-one coordinate mapping by $\pi(i) = (u_i, v_i)$. Each node is associated with a C -dimensional feature vector $x_i \in \mathbb{R}^C$. The proposed GFA block first fixes a global connectivity budget, specified by a target average in-degree \bar{d} or equivalently a total edge budget $B = N\bar{d}$. This budget is then allocated to individual nodes according to their local complexity, yielding node-wise quotas q_i and target degrees d_i^* . Based on these targets, each node selects its neighbors from a dual-scale candidate set that combines local and global samples, after which feature aggregation is performed on the resulting directed graph. Therefore, the proposed design separates *where to connect* (dual-scale candidate sampling) from *how much to connect*

(complexity-aware degree budgeting).

The GFA workflow comprises four steps:

- Dual-scale candidate sampling** (§3.3.1): for each node i , we construct a local candidate set $\mathcal{C}_i^{\text{loc}}$ and a global candidate set $\mathcal{C}_i^{\text{glo}}$, yielding a flexible receptive field.
- Complexity-aware degree budgeting** (§3.3.2): each node is assigned a *neighbor quota* q_i that specifies its target in-degree.
- Graph construction** (§3.3.3): given \mathcal{C}_i and q_i , node i selects its connected neighbors via per-node thresholding on cosine similarity, resulting in a directed adjacency A .
- Graph aggregation** (§3.3.4): features are updated by edge-conditioned aggregation with dual-graphs.

We model the feature map as a *directed* graph $\mathcal{G} = (\mathcal{V}, \mathcal{E})$, where $\mathcal{V} = \{1, \dots, N\}$ refers to vertices and a directed edge $j \rightarrow i$ indicates that j contributes a message to the update of i . For efficiency, each node first constructs a candidate set $\mathcal{C}_i \subseteq \mathcal{V}$ and then selects a subset $\mathcal{N}_i \subseteq \mathcal{C}_i$ with size $d_i \triangleq |\mathcal{N}_i|$ for feature aggregation.

3.3.1. Flexible Receptive Fields via Dual-scale Sampling

The spatial footprint of candidate set \mathcal{C}_i shapes the receptive field of node i . To avoid $O(N^2)$ global pairwise computations of similarities to select neighbors, we adopt a *dual-scale* sampling scheme whose per-node cost is near-linear in the number of samples, while approximately expanding the effective receptive field to the full image.

Dense local sampling. We collect candidates within a fixed-size neighborhood centered, similar to CNN and window attention, which captures fine-grained local structure crucial for low-level vision. Let $L \in \mathbb{N}$ be the local window size.

For $\pi(i) = (u_i, v_i)$, we define the local candidate set as

$$C_i^{\text{loc}} = \{j \in \mathcal{V} \mid \pi(j) = (u_i + \Delta_u, v_i + \Delta_v), \Delta_u, \Delta_v \in \mathbb{Z}, |\Delta_u|, |\Delta_v| \leq \frac{L-1}{2}\}, \quad (1)$$

Sparse global sampling. We introduce a mesh-grid sampling scheme inspired by dilated convolutions and stride sampling [25, 42, 77, 83]. Unlike the approach in [66] that relies on a fixed set of global anchors, we generate per-node mesh-grids, activating more pixels for global interactions.

Let $G \in \mathbb{N}$ be the grid size. Define strides $\Omega_h = \lfloor H/G \rfloor$ and $\Omega_w = \lfloor W/G \rfloor$. We place a $G \times G$ mesh centered at $\pi(i)$ by recording its position within the stride lattice via $r_i \equiv u_i \bmod \Omega_h$ and $c_i \equiv v_i \bmod \Omega_w$. The global candidate set is the lattice points aligned with (r_i, c_i) :

$$C_i^{\text{glo}} = \{j \in \mathcal{V} \mid \pi(j) = (r_i + u\Omega_h, c_i + v\Omega_w), u \in \{0, \dots, G-1\}, v \in \{0, \dots, G-1\}\}, \quad (2)$$

Dense local sampling captures fine structures while sparse global sampling contributes long-range context, yielding an adaptive receptive field without quadratic cost.

3.3.2. Complexity-aware Neighbor Quota Assignment

Node degrees need not be fixed in a GNN. We allocate each node a target in-degree (quota) proportional to a pixel-wise complexity score. Intuitively, pixels with larger local variation are harder to compress and should attend to more neighbors to aggregate information for removing redundancy. We propose to use Sobel operator [63] to calculate gradients and assess the local complexity of each feature pixel.

RMS-Gradient (RMS-G) complexity scoring. Using the 3×3 Sobel filters K_x, K_y , we compute per-channel gradients

$$S_{x,c} = F_c * K_x, \quad S_{y,c} = F_c * K_y, \quad c = 1, \dots, C, \quad (3)$$

and define the magnitude and the cross-channel Root Mean Square (RMS) score at coordinate (u, v) as

$$|\nabla F_c(u, v)| = \sqrt{S_{x,c}(u, v)^2 + S_{y,c}(u, v)^2}, \quad (4)$$

$$s(u, v) = \sqrt{\frac{1}{C} \sum_{c=1}^C |\nabla F_c(u, v)|^2}. \quad (5)$$

Let $s_i \triangleq s(\pi(i)) \geq 0$. Compared with down/up-sampling residual proxies [66], Sobel directly measures first-order spatial variation and emphasizes large local changes (edges, fine details), which typically correlate with coding difficulty. Moreover, since RMS is sensitive to larger values, it better captures the energy compaction phenomenon [38] compared to the simple averaging strategy used by [66]. Further discussion of this choice is provided in the supplementary material.

From global budget to per-node quotas. Let \bar{d} be the target average in-degree and $B \triangleq N \bar{d}$ the total edge budget. We

convert $\{s_i\}$ into normalized weights $w_i = \frac{s_i}{\sum_{k=1}^N s_k}$, and allocate real-valued quotas $q_i = B w_i$. The target degree is

$$d_i^* = \text{clip}(\text{round}(q_i), 1, n_i), \quad (6)$$

ensuring at least one neighbor and at most all candidates.

3.3.3. Graph Construction

The primary redundancy lies among content-similar pixels. To promote redundancy removal, each node should connect to content-correlated candidates by thresholding cosine similarity. For node features $x_i, x_j \in \mathbb{R}^C$, define

$$S_{ij} = \frac{\langle x_i, x_j \rangle}{\|x_i\|_2 \|x_j\|_2}, \quad j \in C_i. \quad (7)$$

We seek a per-node threshold θ_i such that the selected count

$$m_i(\theta_i) \triangleq \#\{j \in C_i : S_{ij} \geq \theta_i\} \approx d_i^*, \quad (8)$$

where $\#\{\cdot\}$ denotes set cardinality. The resulting directed neighborhood and determined adjacency are

$$\mathcal{N}_i = \{j \in C_i : S_{ij} \geq \theta_i\}, A_{ij} = \begin{cases} 1, & \text{if } j \in \mathcal{N}_i, \\ 0, & \text{otherwise.} \end{cases} \quad (9)$$

Per-node bisection for θ_i . We solve $m_i(\theta_i) \approx d_i^*$ via a few iterations of bisection. Let $\ell_i = \min_{j \in C_i} S_{ij}$, $u_i = \max_{j \in C_i} S_{ij}$, we initialize $\theta_i = \frac{1}{n_i} \sum_{j \in C_i} S_{ij}$. Each iteration halves the feasible interval, yielding near-linear cost in n_i . Detailed algorithm is provided below.

Algorithm 1 Per-node threshold searching via bisection

- 1: **Input:** features $\{x_i\}_{i=1}^N$, candidates $\{C_i\}$, targets $\{d_i^*\}$, iterations T
 - 2: **Output:** adjacency $A \in \{0, 1\}^{N \times N}$
 - 3: Compute S_{ij} for all i and $j \in C_i$ (cosine similarity)
 - 4: **for** each node i **in parallel do**
 - 5: $\ell_i \leftarrow \min_{j \in C_i} S_{ij}$; $u_i \leftarrow \max_{j \in C_i} S_{ij}$; $\theta_i \leftarrow \frac{1}{|C_i|} \sum_{j \in C_i} S_{ij}$
 - 6: **for** $t = 1$ **to** T **do**
 - 7: $m_i \leftarrow \#\{j \in C_i : S_{ij} \geq \theta_i\}$
 - 8: **if** $m_i > d_i^*$ **then**
 - 9: $\ell_i \leftarrow \theta_i$
 - 10: **else**
 - 11: $u_i \leftarrow \theta_i$
 - 12: **end if**
 - 13: $\theta_i \leftarrow (\ell_i + u_i)/2$
 - 14: **end for**
 - 15: $\mathcal{N}_i \leftarrow \{j \in C_i : S_{ij} \geq \theta_i\}$; set $A_{ij} \leftarrow 1$ for $j \in \mathcal{N}_i$ and $A_{ij} \leftarrow 0$ otherwise
 - 16: **end for**
-

Complexity. Per node, similarity evaluation and bisection over T iterations cost $O(n_i + T \log n_i)$ time; in practice with small T and moderate $n_i \approx L^2 + G^2$, this is near-linear.

Table 1. **Connectivity-oriented comparison.** Notation: N denotes the total number of nodes/pixels; k the side length of the convolution kernel; L the side length of the attention/GNN window; and K the average neighborhood size (connectivity and in-degrees for GNNs). Computational cost is reported as *construction + aggregation*. “Construction” counts candidate search and similarity calculation.

Method	Candidates	Selection & Degree	Receptive Field	Complexity
<i>Canonical operators</i>				
Dynamic CNN	$k \times k$ window	keep-all; degree = k^2	bounded by window	$\mathcal{O}(1) + \mathcal{O}(Nk^2)$
Deformable CNN	offset-enlarged $k \times k$ window	keep-all; degree = k^2	offset-enlarged local window	$\mathcal{O}(Nk) + \mathcal{O}(Nk)$
Window Attention	$L \times L$ window	keep-all; degree = L^2	bounded by window	$\mathcal{O}(1) + \mathcal{O}(NL^2)$
Transformer (global)	all nodes	keep-all; degree = N	full	$\mathcal{O}(1) + \mathcal{O}(N^2)$
<i>GNN-based LIC</i>				
Fully-connected GAT [65]	all nodes	keep-all; degree = $N-1$	full	$\mathcal{O}(1) + \mathcal{O}(N^2)$
Global k NN GNN [75]	all nodes	k NN; degree = K	full	$\mathcal{O}(N^2) + \mathcal{O}(NK)$
Window k NN GAT [64]	$L \times L$ window	k NN; degree = K	bounded by window	$\mathcal{O}(NL^2) + \mathcal{O}(NK)$
GLIC (ours)	local window \cup sparse global grid (n candidates in total)	per-node threshold and adaptive degree quota; average degree K	near-full	$\mathcal{O}(Nn) + \mathcal{O}(NK)$

3.3.4. Graph Aggregation

Following edge-conditioned aggregation [62, 66, 83], we update node features over the constructed directed graphs. Let $z_i^\ell \in \mathbb{R}^{C_\ell}$ be the feature of node i at layer ℓ . We compute

$$z_i^\ell = \sum_{j \in \mathcal{N}_i} \alpha_{i \leftarrow j}^\ell \phi^\ell(z_j^{\ell-1}), \quad (10)$$

$$\alpha_{i \leftarrow j}^\ell = \frac{\exp(g^\ell(z_i^{\ell-1}, z_j^{\ell-1}))}{\sum_{u \in \mathcal{N}_i} \exp(g^\ell(z_i^{\ell-1}, z_u^{\ell-1}))}. \quad (11)$$

where ϕ^ℓ is a learnable linear projection and g^ℓ is cosine similarity. This design prioritizes pairwise pixel relations and preserves contextual information across both analysis and synthesis transforms.

3.4. Connectivity Comparisons

In this section we compare the connectivity pattern and complexity of canonical operators and prior GNN-based LIC models (Table 1). Dynamic and deformable CNNs as well as window-based attention and window-based GAT restrict connections to local or window-bounded regions, thereby missing truly global redundancy, while global Transformers and fully-connected GATs achieve full receptive fields at the cost of quadratic complexity $\mathcal{O}(N^2)$. In contrast, our GLIC constructs dual-scale graphs with a small candidate set and adaptive degree, attaining a near-global receptive field while keeping both graph construction and aggregation linear in N (i.e., $\mathcal{O}(Nn)$ and $\mathcal{O}(NK)$), which achieves near-full global connectivity without quadratic overhead.

4. Experiments

4.1. Experimental Setup

4.1.1. Training Details

We train GLIC models on the Flickr2W dataset [46]. Models are optimized with Adam [33] with an initial learning rate of 0.0001. We adopt the training acceleration strategy introduced by [38], reducing the total training time to 3 days. To measure the distortion, we employ mean square error

(MSE) and multiscale structural similarity (MS-SSIM). For MSE-optimized models, we set Lagrangian multipliers λ as $\{0.0017, 0.0035, 0.0067, 0.0130, 0.0250, 0.050\}$; for MS-SSIM-optimized models, we set $\{3, 5, 8, 16, 36, 64\}$. All experiments are conducted on NVIDIA A100 GPUs.

4.1.2. Evaluation

We evaluate our models on three datasets: the Kodak image set [34] with a resolution of 768×512 , the Tecnick test set [2] with a resolution of 1200×1200 , and the CLIC2020Val dataset [69] with 2K resolution. For RD performance evaluation, we employ PSNR, MS-SSIM, and bits per pixel (bpp) as the key metrics. We use BD-rate [6] to measure the average bitrate savings. We also use BD-PSNR to measure the average PSNR gain at the same bitrates. For model complexity, we utilize parameter count, FLOPs, encoding/decoding latency and peak memory for 2K images as metrics.

4.1.3. Model Details

We set channel numbers $\{C_1, C_2, C_3, C_4\}$ as $\{128, 192, 192, 320\}$ and transform block numbers $\{L_1, L_2, L_3\}$ as $\{3, 5, 5\}$. We employ SCCTX model [27] with 5 slices for entropy coding. The dense sampling size is set as 8 and sparse sampling size is 16. We set the average node degree as 64.

4.2. Rate-Distortion Performance

We benchmark our method against the traditional image codec VTM-9.1 [7], as well as several SOTA LIC methods including FTIC [37], CCA [23], WeConvene [19], HPCM [43], LALIC [15], DCAE [50], MambaIC [79]. The resulting RD curves, depicted in Fig. 3-5, illustrate the performance trends across different bit rates. Detailed BD-rate comparisons, with VTM-9.1 as the anchor, are reported in Tab. 2. Our GLIC model outperforms VTM-9.1 by -19.29%, and -21.69%, -18.71% in BD-rate on Kodak, Tecnick, and CLIC datasets, significantly surpassing previous methods.

Specifically, in terms of BD-PSNR improvements, when compared with FTIC [37], our method achieves gains of 0.26 dB, 0.37 dB, and 0.38 dB on the Kodak, CLIC, and Tecnick datasets, respectively. Furthermore, the improvements become even more pronounced against TCM-L [47],

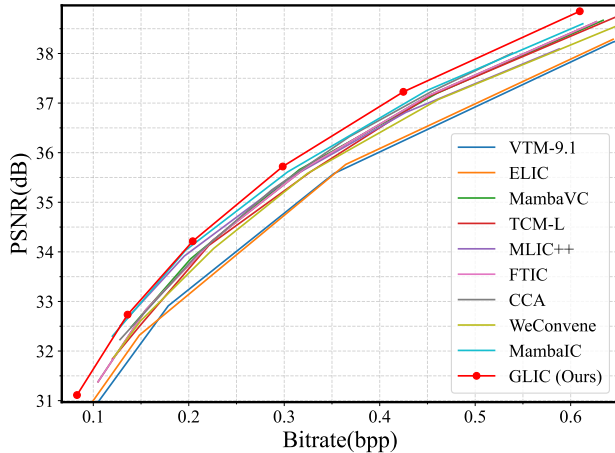


Figure 3. PSNR R-D curves on the CLIC 2020 dataset.

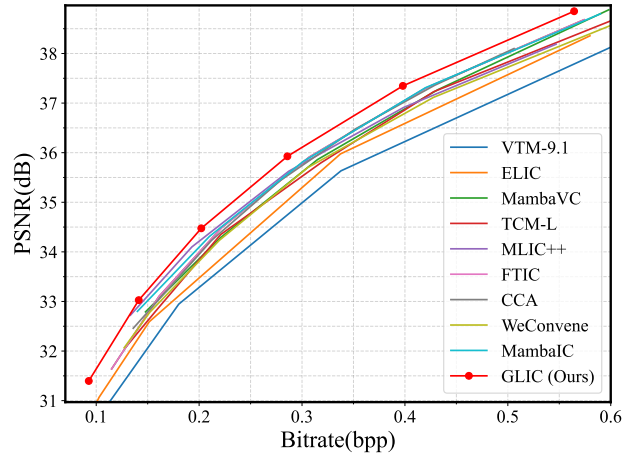


Figure 4. PSNR R-D curves on the Tecnick dataset.

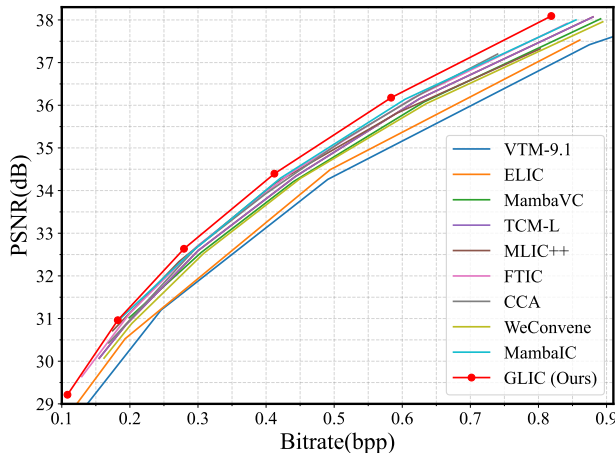
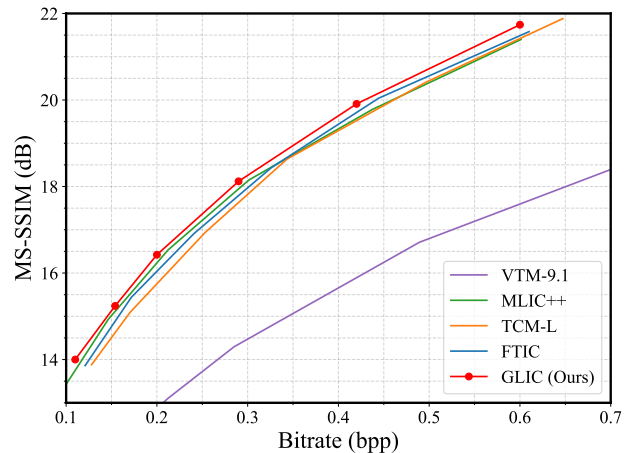


Figure 5. PSNR and MS-SSIM R-D curves on the Kodak Dataset.



with BD-PSNR increases of 0.39 dB, 0.46 dB, and 0.56 dB on the corresponding datasets. In terms of MS-SSIM, our GLIC model also achieves 0.46 dB and 0.28 dB improvements on the CLIC dataset compared to TCM-L and FTIC, respectively, as shown in Fig. 5. These results not only demonstrate the robustness of our approach but also validate its superiority across a variety of resolutions.

4.3. Effective Receptive Fields

We visualize the effective receptive fields (ERFs) [52] of LIC models to demonstrate the superiority of our method. We first show the averaged ERF on the Kodak dataset in Fig. 6. In these visualizations, a larger ERF appears as a broader spread of dark regions. Compared with prior methods, our GLIC model exhibits a substantially larger ERF, attributable to its dual-graph strategy, which adaptively captures long-range dependencies within images.

Single-image ERF. We also present single-image ERF visualizations (Fig. 6) using Kodak image 23. ERFs are computed from two locations in the latent feature map: the center and a point slightly to its right (details of the ERF computation are provided in the supplementary material). Although

these points are close in space, one lies in the background and the other on the foreground parrot. Prior models produce ERFs with similar, mildly isotropic shapes at both locations. In contrast, our method yields clearly different, content-aware ERFs: for the central background point, the ERF concentrates on background regions (especially the blades of grass), largely skipping the nearby parrot. For the foreground point on the parrot, despite its Euclidean proximity to the first point, the ERF focuses on the red feathers of the right parrot. These results align with human perception of redundancy and semantic structure, indicating that our model performs content-adaptive redundancy detection and elimination. This is a dynamic behavior absent from existing methods, highlighting the advantage of our approach.

4.4. Computational Complexity

Beyond RD performance, we evaluate computational complexity on 2K-resolution images by reporting parameter count, forward FLOPs, decoding latency, and peak memory on an A100 GPU with an AMD EPYC 7742 64-core CPU, as summarized in Tab. 2. GLIC attains a markedly better efficiency-latency trade-off than recent SOTA codecs. Com-

Table 2. **Quantitative Comparisons of leading LIC methods.** BD-rates are evaluated against VTM-9.1. FLOPs, peak memory and decoding time are measured on 2K-resolution images.

Method	Complexity					BD-rate (%) ↓		
	Params (M)	FLOPs (T)	Enc-Lat. (s)	Dec-Lat. (s)	Peak-Mem. (G)	Kodak	Tecnick	CLIC
VTM-9.1 [7]	-	-	-	-	-	0.00	0.00	0.00
ELIC (CVPR'22) [27]	33.29	1.74	0.583	0.335	1.50	-5.95	-7.68	-1.20
MLIC++ (ICML'23W) [28]	116.48	2.64	0.508	0.547	2.08	-15.14	-17.23	-14.41
TCM-L (CVPR'23) [47]	75.89	3.74	0.647	0.542	7.73	-13.42	-10.93	-9.10
FTIC (ICLR'24) [37]	69.78	2.38	>10	>10	4.90	-14.83	-14.39	-10.70
CCA (NeurIPS'24) [23]	64.89	3.28	0.526	0.385	5.04	-13.94	-14.13	-11.93
WeConvne (ECCV'24) [19]	105.51	4.82	1.264	1.293	4.53	-8.96	-10.70	-7.55
HPCM (ICCV'25) [43]	68.50	2.00	0.532	0.498	5.89	-16.13	-17.26	-15.02
DCAE (CVPR'25) [50]	119.22	2.28	0.428	0.449	5.59	-17.18	-20.07	-16.91
LALIC (CVPR'25) [15]	63.24	2.53	0.779	0.362	3.89	-15.50	-17.71	-15.47
MambaIC (CVPR'25) [79]	157.09	5.56	1.436	0.669	20.32	-15.13	-15.78	-15.73
GLIC (Ours)	67.20	2.48	0.617	0.395	5.46	-19.29	-21.69	-18.71

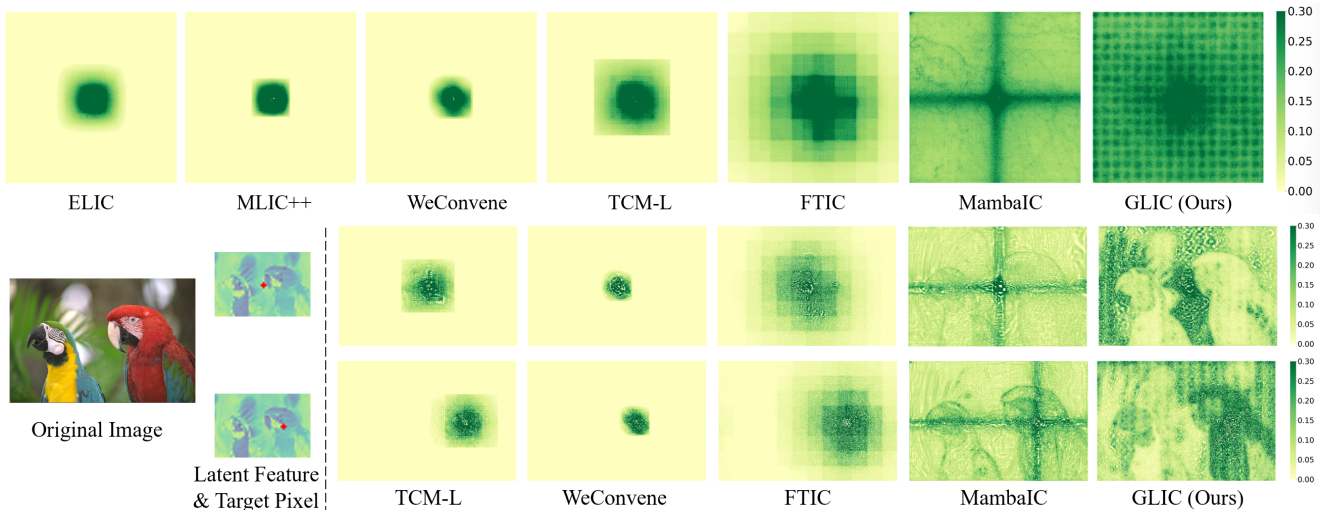


Figure 6. (Top) Averaged Effective Receptive Fields of state-of-the-art LIC models across the 24 Kodak images. (Bottom) Single-image Effective Receptive Field for Kodak image 23, demonstrating the adaptivity of our GLIC model. More results are in the supplementary.

pared with recent SOTA methods MambaIC [79] (CVPR25), GLIC reduces parameter count, FLOPs, decoding latency and peak memory by 57.2%, 55.4%, 41.0%, and 73.1%, respectively. Relative to WeConvne, GLIC further reduces parameters by 36.3%, FLOPs by 48.5%, and decoding latency by 69.5%. Compared with FTIC, it achieves substantially lower decoding latency with a similar parameter budget. These efficiency gains are obtained without sacrificing SOTA RD performance, indicating that the proposed GNN-based Feature Aggregation block effectively balances compression performance and computational cost.

Computational overhead during graph construction. We use $T = 5$ iterations in Algorithm 1 for graph construction. The updates are implemented with matrix operations and run in parallel over all nodes, so the overhead is small. The 5-iteration update accounts for about 5% of the training time. At test time, the additional encoding and decoding latency on 2K images is below 0.02s (less than 5% of the encoding/decoding times), confirming the efficiency of our

bisection-based graph construction method.

4.5. Illustration of RMS-G Scores

We visualize the per-node RMS-G scores in Fig. 7. Brighter colors indicate higher RMS-G values, corresponding to structurally complex, hard-to-compress regions that are assigned larger target degrees. In contrast, smooth background areas exhibit lower RMS-G values and thus receive fewer neighbors. Overall, the RMS-G map closely follows human perception by emphasizing high-frequency, texture-rich content where spatial redundancy is limited.

4.6. Ablation Studies

Dual-scale Graph Design. Tab. 3 studies the effect of the local and global graphs. Using only the local graph or only the global graph leads to clear RD degradation on all three datasets. The global-only variant is the weakest, showing that local aggregation is still necessary. The “Reverse” setting, which flips the order of local and global aggregation, is better than the single-branch variants but remains worse than

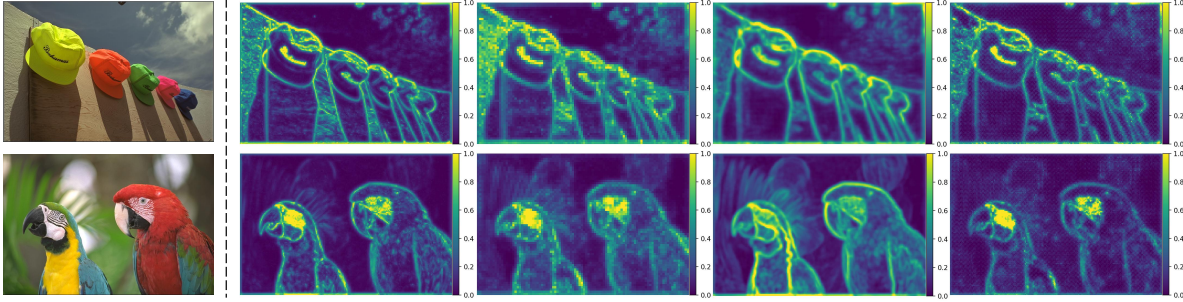


Figure 7. **Spatial redundancy versus RMS-G scores.** Image023 from the Kodak dataset (left) and the RMS-G maps for the second- and third-stage graphs in GLIC (right). Brighter regions have higher RMS-G scores, indicating lower spatial redundancy and larger in-degrees.



Figure 8. Visual Comparisons with other methods. More results are in the supplementary.

Table 3. Ablations on dual-scale graph flexibility.

Variant	Kodak	CLIC	Tecnick
w/o Global (Local only)	-16.98	-15.71	-18.89
w/o Local (Global only)	-15.62	-15.02	-17.51
Reverse (Local+Global)	-18.77	-18.21	-20.79
Global+Local (Ours)	-19.29	-18.71	-21.69

our design. The full “Global+Local” configuration achieves the best BD-rates, especially on Tecnick, indicating that combining local details and long-range context in the proposed order is important for high-resolution images.

Complexity-aware Scoring and Pooling. Tab. 4 evaluates different complexity scores and channel pooling strategies. The row “None / None” disables complexity assessment, turning the model into a k NN-based GNN, which yields the weakest BD-rates. Introducing any complexity score already brings consistent gains, and both Rescaling Residual and Sobel Gradient outperform local entropy. Within the same score, channel pooling also matters: for Sobel Gradient, RMS pooling clearly improves over mean pooling on all three datasets. The combination of Sobel Gradient and RMS pooling gives the strongest RD performance, and is therefore adopted as our default complexity measure.

4.7. Visual Comparisons

In Fig. 8, we visually compare our GLIC model with the traditional codec VTM-9.1 [7] and LIC model TCM [47]. A detailed comparison of image patches reveals that our GLIC model better preserves high-frequency details and textures, effectively mitigating the severe detail loss and over-

Table 4. Ablations on complexity scoring and channel pooling.

Scoring Strategy	Channel Pooling	Kodak	CLIC	Tecnick
None	None	-16.97	-16.21	-18.21
Local Entropy	RMS	-17.05	-17.01	-18.97
Rescaling Residual	RMS	-17.67	-17.03	-19.68
Rescaling Residual	Mean	-18.23	-17.82	-20.39
Sobel Gradient	Mean	-18.02	-17.42	-20.62
Sobel Gradient	RMS	-19.29	-18.71	-21.69

smoothing observed in other methods. This improvement stems from our complexity-aware neighbor quota assignment mechanism, which adaptively allocates more connections to complex regions for enhanced feature aggregation.

More visualizations, ablations and discussions about limitations are provided in the supplementary.

5. Conclusion

We address the limitation that standard CNN kernels and window-based attention are inherently rigid. They impose fixed receptive fields and static connectivity that can couple uncorrelated features within the same Euclidean neighborhood and hinder adaptation to spatially varying redundancy. To overcome this, we propose GLIC, a content-adaptive LIC framework that builds dual-scale graphs and employs a complexity-aware scoring mechanism to enable flexible receptive fields and pixel-wise adaptive connectivity with linear complexity. Extensive experiments demonstrate state-of-the-art rate-distortion performance, validating the strong potential and effectiveness of graph-based, content-adaptive redundancy modeling for image compression.

Acknowledgment

This work was supported by the National Key Research and Development Program of China under Grant 2024YFF0509700, National Natural Science Foundation of China (62471290,62431015,62331014,62501337) and the Fundamental Research Funds for the Central Universities.

References

- [1] Pinar Akyazi and Touradj Ebrahimi. Learning-based image compression using convolutional autoencoder and wavelet decomposition. In *IEEE Conference on Computer Vision and Pattern Recognition Workshops*, 2019. 2
- [2] Nicola Asuni, Andrea Giachetti, et al. Testimages: a large-scale archive for testing visual devices and basic image processing algorithms. In *STAG*, pages 63–70, 2014. 5
- [3] Johannes Ballé, Valero Laparra, and Eero P. Simoncelli. End-to-end optimized image compression. In *International Conference on Learning Representations*, 2017. 1, 2
- [4] Johannes Ballé, David Minnen, Saurabh Singh, Sung Jin Hwang, and Nick Johnston. Variational image compression with a scale hyperprior. In *International Conference on Learning Representations*, 2018. 1, 2
- [5] Jean Bégaint, Fabien Racapé, Simon Feltman, and Akshay Pushparaja. Compressai: a pytorch library and evaluation platform for end-to-end compression research. *arXiv e-prints*, pages arXiv–2011, 2020. 2
- [6] Gisle Bjontegaard. Calculation of average psnr differences between rd-curves. In *VCEG-M33*, 2001. 5
- [7] Benjamin Bross, Ye-Kui Wang, Yan Ye, Shan Liu, Jianle Chen, Gary J Sullivan, and Jens-Rainer Ohm. Overview of the versatile video coding (vvc) standard and its applications. *IEEE Transactions on Circuits and Systems for Video Technology*, 31(10):3736–3764, 2021. 5, 7, 8
- [8] Fangdong Chen, Yumeng Xu, and Li Wang. Two-stage octave residual network for end-to-end image compression. In *Proceedings of the AAAI Conference on Artificial Intelligence*, pages 3922–3929, 2022. 2
- [9] Yunuo Chen, Qian Li, Bing He, Donghui Feng, Ronghua Wu, Qi Wang, Li Song, Guo Lu, and Wenjun Zhang. S2cformer: Reorienting learned image compression from spatial interaction to channel aggregation, 2025. 1, 2
- [10] Yunuo Chen, Zezheng Lyu, Bing He, Ning Cao, Gang Chen, Guo Lu, and Wenjun Zhang. Knowledge distillation for learned image compression. In *Proceedings of the IEEE/CVF International Conference on Computer Vision*, pages 4996–5006, 2025. 1
- [11] Yunuo Chen, Zezheng Lyu, Bing He, Hongwei Hu, Qi Wang, Yuan Tian, Li Song, Wenjun Zhang, and Guo Lu. Content-aware mamba for learned image compression. In *The Fourteenth International Conference on Learning Representations*, 2026. 2
- [12] Yunuo Chen, Chuqin Zhou, Jiangchuan Li, Xiaoyue Ling, Bing He, Jincheng Dai, Li Song, and Guo Lu. Next-frame decoding for ultra-low-bitrate image compression with video diffusion priors. *arXiv preprint arXiv:2603.15129*, 2026. 2
- [13] Zhengxue Cheng, Heming Sun, Masaru Takeuchi, and Jiro Katto. Learned image compression with discretized gaussian mixture likelihoods and attention modules. In *Proceedings of the IEEE/CVF conference on computer vision and pattern recognition*, pages 7939–7948, 2020. 2
- [14] Junhao Du, Chuqin Zhou, Ning Cao, Gang Chen, Yunuo Chen, Zhengxue Cheng, Li Song, Guo Lu, and Wenjun Zhang. Large language model for lossless image compression with visual prompts. *arXiv preprint arXiv:2502.16163*, 2025. 2
- [15] Donghui Feng, Zhengxue Cheng, Shen Wang, Ronghua Wu, Hongwei Hu, Guo Lu, and Li Song. Linear attention modeling for learned image compression. In *Proceedings of the Computer Vision and Pattern Recognition Conference*, pages 7623–7632, 2025. 5, 7
- [16] Haisheng Fu and Feng Liang. Learned image compression with generalized octave convolution and cross-resolution parameter estimation. *Signal Processing*, 202:108778, 2023. 2
- [17] Haisheng Fu, Feng Liang, Jie Liang, Binglin Li, Guohe Zhang, and Jingning Han. Asymmetric learned image compression with multi-scale residual block, importance scaling, and post-quantization filtering. *IEEE Transactions on Circuits and Systems for Video Technology*, 33(8):4309–4321, 2023. 2
- [18] Haisheng Fu, Feng Liang, Jie Liang, Yongqiang Wang, Zhenman Fang, Guohe Zhang, and Jingning Han. Fast and high-performance learned image compression with improved checkerboard context model, deformable residual module, and knowledge distillation. *IEEE Transactions on Image Processing*, 2024. 2
- [19] Haisheng Fu, Jie Liang, Zhenman Fang, Jingning Han, Feng Liang, and Guohe Zhang. Weconvene: Learned image compression with wavelet-domain convolution and entropy model. In *European Conference on Computer Vision*, pages 37–53. Springer, 2024. 2, 5, 7
- [20] Ge Gao, Pei You, Rong Pan, Shunyu Han, Yuanyuan Zhang, Yuchao Dai, and Hojae Lee. Neural image compression via attentional multi-scale back projection and frequency decomposition. In *Proceedings of the IEEE/CVF International Conference on Computer Vision*, pages 14677–14686, 2021. 2
- [21] Marco Gori, Gabriele Monfardini, and Franco Scarselli. A new model for learning in graph domains. In *Proceedings. 2005 IEEE international joint conference on neural networks, 2005.*, pages 729–734. IEEE, 2005. 2
- [22] Kai Han, Yunhe Wang, Jianyuan Guo, Yehui Tang, and Enhua Wu. Vision gnn: An image is worth graph of nodes. *Advances in neural information processing systems*, 35:8291–8303, 2022. 2
- [23] Minghao Han, Shiyin Jiang, Shengxi Li, Xin Deng, Mai Xu, Ce Zhu, and Shuhang Gu. Causal context adjustment loss for learned image compression. In *The Thirty-eighth Annual Conference on Neural Information Processing Systems*, 2024. 5, 7
- [24] Yan Han, Peihao Wang, Souvik Kundu, Ying Ding, and Zhangyang Wang. Vision hgnn: An image is more than a graph of nodes. In *Proceedings of the IEEE/CVF International Conference on Computer Vision*, pages 19878–19888, 2023. 2

- [25] Ali Hassani and Humphrey Shi. Dilated neighborhood attention transformer, 2023. 4
- [26] Dailan He, Yaoyan Zheng, Baocheng Sun, Yan Wang, and Hongwei Qin. Checkerboard context model for efficient learned image compression. In *Proceedings of the IEEE/CVF Conference on Computer Vision and Pattern Recognition*, pages 14771–14780, 2021. 2
- [27] Dailan He, Ziming Yang, Weikun Peng, Rui Ma, Hongwei Qin, and Yan Wang. Elic: Efficient learned image compression with unevenly grouped space-channel contextual adaptive coding. In *Proceedings of the IEEE/CVF Conference on Computer Vision and Pattern Recognition*, pages 5718–5727, 2022. 5, 7
- [28] Wei Jiang and Ronggang Wang. MLIC++: Linear complexity multi-reference entropy modeling for learned image compression. In *ICML 2023 Workshop Neural Compression: From Information Theory to Applications*, 2023. 1, 7
- [29] Wei Jiang, Jiayu Yang, Yongqi Zhai, Peirong Ning, Feng Gao, and Ronggang Wang. Mlic: Multi-reference entropy model for learned image compression. In *Proceedings of the 31st ACM International Conference on Multimedia*, pages 7618–7627, 2023. 1, 2
- [30] Wei Jiang, Peirong Ning, Jiayu Yang, Yongqi Zhai, Feng Gao, and Ronggang Wang. Llic: Large receptive field transform coding with adaptive weights for learned image compression. *IEEE Transactions on Multimedia*, 26:10937–10951, 2024. 2
- [31] Wei Jiang, Yongqi Zhai, Jiayu Yang, Feng Gao, and Ronggang Wang. Mlicv2: Enhanced multi-reference entropy modeling for learned image compression. *arXiv preprint arXiv:2504.19119*, 2025. 2
- [32] Yongcheng Jing, Yining Mao, Yiding Yang, Yibing Zhan, Mingli Song, Xinchao Wang, and Dacheng Tao. Learning graph neural networks for image style transfer. In *European Conference on Computer Vision*, pages 111–128. Springer, 2022. 2
- [33] Diederik P Kingma. Adam: A method for stochastic optimization. *International Conference on Learning Representations*, 2015. 5
- [34] Eastman Kodak. Kodak lossless true color image suite (photocd pcd0992), 1993. Available from <http://r0k.us/graphics/kodak/>. 5
- [35] Loic Landrieu and Martin Simonovsky. Large-scale point cloud semantic segmentation with superpoint graphs. In *Proceedings of the IEEE conference on computer vision and pattern recognition*, pages 4558–4567, 2018. 2
- [36] Daowen Li, Yingming Li, Heming Sun, and Lu Yu. Deep image compression based on multi-scale deformable convolution. *Journal of Visual Communication and Image Representation*, 87:103573, 2022. 2
- [37] Han Li, Shaohui Li, Wenrui Dai, Chenglin Li, Junni Zou, and Hongkai Xiong. Frequency-aware transformer for learned image compression. In *The Twelfth International Conference on Learning Representations*, 2024. 1, 2, 5, 7
- [38] Han Li, Shaohui Li, Wenrui Dai, Maida Cao, Nuowen Kan, Chenglin Li, Junni Zou, and Hongkai Xiong. On disentangled training for nonlinear transform in learned image compression. In *The Thirteenth International Conference on Learning Representations*, 2025. 1, 4, 5
- [39] Jiahao Li, Bin Li, and Yan Lu. Hybrid spatial-temporal entropy modelling for neural video compression. In *Proceedings of the 30th ACM International Conference on Multimedia*, pages 1503–1511, 2022. 2
- [40] Jiahao Li, Bin Li, and Yan Lu. Neural video compression with diverse contexts. In *Proceedings of the IEEE/CVF Conference on Computer Vision and Pattern Recognition*, pages 22616–22626, 2023. 2
- [41] Jiangchuan Li, Chuqin Zhou, Yunuo Chen, and Guo Lu. Differentiable vmf: A trainable metric for optimizing video compression codec. In *2025 IEEE International Symposium on Circuits and Systems (ISCAS)*, pages 1–5. IEEE, 2025. 1
- [42] Yao Li, Xueyang Fu, and Zheng-Jun Zha. Cross-patch graph convolutional network for image denoising. In *Proceedings of the IEEE/CVF International Conference on Computer Vision*, pages 4651–4660, 2021. 2, 4
- [43] Yuqi Li, Haotian Zhang, Li Li, and Dong Liu. Learned image compression with hierarchical progressive context modeling. *arXiv preprint arXiv:2507.19125*, 2025. 5, 7
- [44] Huanxiong Liang, Yunuo Chen, Yicheng Pan, Sixian Wang, Jincheng Dai, Guo Lu, and Wenjun Zhang. Structure-guided allocation of 2d gaussians for image representation and compression. *arXiv preprint arXiv:2512.24018*, 2025. 2
- [45] Xiaoyue Ling, Chuqin Zhou, Chunyi Li, Yunuo Chen, Yuan Tian, Guo Lu, and Wenjun Zhang. Free-gvc: Towards training-free extreme generative video compression with temporal coherence. *arXiv preprint arXiv:2602.09868*, 2026. 2
- [46] Jiaheng Liu, Guo Lu, Zhihao Hu, and Dong Xu. A unified end-to-end framework for efficient deep image compression. *arXiv preprint arXiv:2002.03370*, 2020. 5
- [47] Jinming Liu, Heming Sun, and Jiro Katto. Learned image compression with mixed transformer-cnn architectures. In *Proceedings of the IEEE/CVF conference on computer vision and pattern recognition*, pages 14388–14397, 2023. 1, 2, 5, 7, 8
- [48] Ziyu Liu, Ruyi Feng, Lizhe Wang, Wei Han, and Tiejong Zeng. Dual learning-based graph neural network for remote sensing image super-resolution. *IEEE Transactions on Geoscience and Remote Sensing*, 60:1–14, 2022. 2
- [49] Guo Lu, Jing Wang, Yunuo Chen, Chuqin Zhou, Yibo Shi, and Kai Lin. Vcip 2025 ultra low-bitrate video compression challenge. In *2025 International Conference on Visual Communications and Image Processing (VCIP)*, pages 1–3. IEEE, 2025. 2
- [50] Jingbo Lu, Leheng Zhang, Xingyu Zhou, Mu Li, Wen Li, and Shuhang Gu. Learned image compression with dictionary-based entropy model. In *Proceedings of the Computer Vision and Pattern Recognition Conference*, pages 12850–12859, 2025. 5, 7
- [51] Ming Lu, Peiyao Guo, Huiqing Shi, Chuntong Cao, and Zhan Ma. Transformer-based image compression. In *2022 Data Compression Conference (DCC)*, pages 469–469. IEEE, 2022. 2
- [52] Wenjie Luo, Yujia Li, Raquel Urtasun, and Richard Zemel. Understanding the effective receptive field in deep convolutional neural networks. *Advances in neural information processing systems*, 29, 2016. 6

- [53] Haichuan Ma, Dong Liu, Ruiqin Xiong, and Feng Wu. iwave: Cnn-based wavelet-like transform for image compression. *IEEE Transactions on Multimedia*, 22(7):1667–1679, 2019. 2
- [54] Xu Ma, Yuqian Zhou, Huan Wang, Can Qin, Bin Sun, Chang Liu, and Yun Fu. Image as set of points. In *The Eleventh International Conference on Learning Representations*, 2023. 2
- [55] Fabian Mentzer, George Toderici, David Minnen, Sergi Caelles, Sung Jin Hwang, Mario Lucic, and Eirikur Agustsson. VCT: A video compression transformer. In *Advances in Neural Information Processing Systems*, 2022. 2
- [56] Alessio Micheli. Neural network for graphs: A contextual constructive approach. *IEEE Transactions on Neural Networks*, 20(3):498–511, 2009. 2
- [57] David Minnen and Saurabh Singh. Channel-wise autoregressive entropy models for learned image compression. In *2020 IEEE International Conference on Image Processing (ICIP)*, pages 3339–3343. IEEE, 2020. 1, 2
- [58] David Minnen, Johannes Ballé, and George D Toderici. Joint autoregressive and hierarchical priors for learned image compression. *Advances in neural information processing systems*, 31, 2018. 1, 2
- [59] Chong Mou and Jian Zhang. Graph attention neural network for image restoration. In *2021 IEEE International Conference on Multimedia and Expo (ICME)*, pages 1–6. IEEE, 2021. 2
- [60] Yichen Qian, Ming Lin, Xiuyu Sun, Zhiyu Tan, and Rong Jin. Entroformer: A transformer-based entropy model for learned image compression. In *International Conference on Learning Representations*, 2022. 2
- [61] Shiyu Qin, Jinpeng Wang, Yimin Zhou, Bin Chen, Tianci Luo, Baoyi An, Tao Dai, Shutao Xia, and Yaowei Wang. Mambavc: Learned visual compression with selective state spaces. *arXiv preprint arXiv:2405.15413*, 2024. 2
- [62] Martin Simonovsky and Nikos Komodakis. Dynamic edge-conditioned filters in convolutional neural networks on graphs. In *Proceedings of the IEEE conference on computer vision and pattern recognition*, pages 3693–3702, 2017. 5
- [63] Irwin Sobel, Gary Feldman, et al. A 3x3 isotropic gradient operator for image processing. *a talk at the Stanford Artificial Project in*, 1968:271–272, 1968. 4
- [64] Gabriele Spadaro, Alberto Presta, Enzo Tartaglione, Jhony H Giraldo, Marco Grangetto, and Attilio Fiandrotti. Gabic: Graph-based attention block for image compression. In *2024 IEEE International Conference on Image Processing (ICIP)*, pages 1802–1808. IEEE, 2024. 2, 5
- [65] Zhisen Tang, Hanli Wang, Xiaokai Yi, Yun Zhang, Sam Kwong, and C-C Jay Kuo. Joint graph attention and asymmetric convolutional neural network for deep image compression. *IEEE Transactions on Circuits and Systems for Video Technology*, 33(1):421–433, 2022. 2, 5
- [66] Yuchuan Tian, Hanting Chen, Chao Xu, and Yunhe Wang. Image processing gnn: Breaking rigidity in super-resolution. In *Proceedings of the IEEE/CVF Conference on Computer Vision and Pattern Recognition*, pages 24108–24117, 2024. 2, 4, 5
- [67] Yuan Tian, Guo Lu, Yichao Yan, Guangtao Zhai, Li Chen, and Zhiyong Gao. A coding framework and benchmark towards low-bitrate video understanding. *IEEE Transactions on Pattern Analysis and Machine Intelligence*, 46(8):5852–5872, 2024. 2
- [68] Yuan Tian, Xiaoyue Ling, Cong Geng, Qiang Hu, Guo Lu, and Guangtao Zhai. Smc++: Masked learning of unsupervised video semantic compression. *IEEE Transactions on Pattern Analysis and Machine Intelligence*, 2025. 2
- [69] George Toderici, Wenzhe Shi, Radu Timofte, Lucas Theis, Johannes Balle, Eirikur Agustsson, Nick Johnston, and Fabian Mentzer. Workshop and challenge on learned image compression (clic2020), 2020. 5
- [70] Huairui Wang, Zhenzhong Chen, and Chang Wen Chen. Learned video compression via heterogeneous deformable compensation network. *IEEE Transactions on Multimedia*, 26:1855–1866, 2023. 2
- [71] Siqi Wu, Yinda Chen, Dong Liu, and Zhihai He. Conditional latent coding with learnable synthesized reference for deep image compression. *arXiv preprint arXiv:2502.09971*, 2025. 2
- [72] Yueqi Xie, Ka Leong Cheng, and Qifeng Chen. Enhanced invertible encoding for learned image compression. In *Proceedings of the 29th ACM international conference on multimedia*, pages 162–170, 2021. 2
- [73] Danfei Xu, Yuke Zhu, Christopher B Choy, and Li Fei-Fei. Scene graph generation by iterative message passing. In *Proceedings of the IEEE conference on computer vision and pattern recognition*, pages 5410–5419, 2017. 2
- [74] Sijie Yan, Yuanjun Xiong, and Dahua Lin. Spatial temporal graph convolutional networks for skeleton-based action recognition. In *Proceedings of the AAAI conference on artificial intelligence*, 2018. 2
- [75] Chunhui Yang, Yi Ma, Jiayu Yang, Shiyi Liu, and Ronggang Wang. Graph-convolution network for image compression. In *2021 IEEE International Conference on Image Processing (ICIP)*, pages 2094–2098. IEEE, 2021. 2, 5
- [76] Yiding Yang, Jiayan Qiu, Mingli Song, Dacheng Tao, and Xinchao Wang. Distilling knowledge from graph convolutional networks. In *Proceedings of the IEEE/CVF conference on computer vision and pattern recognition*, pages 7074–7083, 2020. 2
- [77] Fisher Yu and Vladlen Koltun. Multi-scale context aggregation by dilated convolutions. *arXiv preprint arXiv:1511.07122*, 2015. 4
- [78] Ali Zafari, Atefeh Khoshkhahtinat, Piyush Mehta, Mohammad Saeed Ebrahimi Saadabadi, Mohammad Akyash, and Nasser M Nasrabadi. Frequency disentangled features in neural image compression. In *2023 IEEE International Conference on Image Processing (ICIP)*, pages 2815–2819. IEEE, 2023. 2
- [79] Fanhu Zeng, Hao Tang, Yihua Shao, Siyu Chen, Ling Shao, and Yan Wang. Mambaic: State space models for high-performance learned image compression. *arXiv preprint arXiv:2503.12461*, 2025. 2, 5, 7
- [80] Yiwei Zhang, Guo Lu, Yunuo Chen, Shen Wang, Yibo Shi, Jing Wang, and Li Song. Neural rate control for learned video compression. In *The Twelfth International Conference on Learning Representations*, 2023. 1
- [81] Yichi Zhang, Zhihao Duan, Ming Lu, Dandan Ding, Fengqing Zhu, and Zhan Ma. Another way to the top: Exploit contextual

- clustering in learned image coding. In *Proceedings of the AAAI Conference on Artificial Intelligence*, pages 9377–9386, 2024. [2](#)
- [82] Chuqin Zhou, Xiaoyue Ling, Yunuo Chen, Jincheng Dai, Guo Lu, and Wenjun Zhang. Dual-representation image compression at ultra-low bitrates via explicit semantics and implicit textures. *arXiv preprint arXiv:2602.05213*, 2026. [2](#)
- [83] Shangchen Zhou, Jiawei Zhang, Wangmeng Zuo, and Chen Change Loy. Cross-scale internal graph neural network for image super-resolution. *Advances in neural information processing systems*, 33:3499–3509, 2020. [2](#), [4](#), [5](#)
- [84] Yin hao Zhu, Yang Yang, and Taco Cohen. Transformer-based transform coding. In *International Conference on Learning Representations*, 2022. [2](#)
- [85] Renjie Zou, Chunfeng Song, and Zhaoxiang Zhang. The devil is in the details: Window-based attention for image compression. In *Proceedings of the IEEE/CVF conference on computer vision and pattern recognition*, pages 17492–17501, 2022. [2](#)